

Antimicrobial activity of silica coated silicon nano-tubes (SCSNT) and silica coated silicon nano-particles (SCSNP) synthesized by gas phase condensation

Chiti Tank · Sujatha Raman · Sujoy Karan · Suresh Gosavi · Niranjana P. Lalla · Vasant Sathe · Richard Berndt · W. N. Gade · S. V. Bhoraskar · Vikas L. Mathe

Received: 6 July 2012 / Accepted: 16 February 2013 / Published online: 14 March 2013
© Springer Science+Business Media New York 2013

Abstract Silica-coated, silicon nanotubes (SCSNTs) and silica-coated, silicon nanoparticles (SCSNPs) have been synthesized by catalyst-free single-step gas phase condensation using the arc plasma process. Transmission electron microscopy and scanning tunneling microscopy showed that SCSNTs exhibited a wall thickness of less than 1 nm, with an average diameter of 14 nm and a length of several 100 nm. Both nano-structures had a high specific surface area. The present study has demonstrated cheaper, resistance-free and effective antibacterial activity in silica-coated silicon nano-structures, each for two Gram-positive and Gram-negative bacteria. The minimum inhibitory concentration (MIC) was estimated, using the optical densitometric technique, and by determining colony-forming units. The MIC was found to range in the order of micrograms, which is comparable to the reported MIC of metal oxides for these bacteria. SCSNTs were found to be more effective in limiting the growth of multidrug-resistant *Staphylococcus aureus* over SCSNPs at 10 µg/ml (IC 50 = 100 µg/ml).

1 Introduction

Nano-materials, due to their large effective surface area with a potent number of reactive sites, are extensively used in biological applications, which include antimicrobial activities, drug delivery and medical imaging [1, 2]. The study of antimicrobial activity of nano-materials is essential for biological applications, especially to develop antimicrobial medicines [3], and to determine the suitability of a material for antimicrobial surfaces [4]. This is important, as the increasing resistance of microorganisms to multiple antibiotics has fueled the demand for effective, resistance-free, cheaper and biocompatible antimicrobial agents.

Nano-materials provide a novel way to replace antibiotics. Nano-particles, for instance, have been used to reduce skin diseases [1, 5] and to prevent the microbial colonies that form on the surface of devices like endotracheal tubes, catheters and prostheses [6]. Although nano-particles of metal (silver, gold etc.) and some oxides (like TiO₂, ZnO, etc.) show convincing antimicrobial activity, their poor dispersion stability in the organic medium makes it difficult to fabricate polymer composites [7]. The drawback with silver nano-particles lies in the rapid oxidation and ease of agglomeration that changes their reactivity with the environment [8]. Besides this, it is an expensive material and its environmental hazards are a matter of concern [9].

Nano-structures of silica, on the other hand, are preferable over other nano-materials due to its noncorrosive and biocompatible properties. Also, they are chemically stable and not as expensive as silver or gold. The surface of silica structures can be functionalized in many ways that make its integration with polymers easier. Silicon derivatives with polymers have been used as anti-corrosive and chemically resistant coatings [10]. Nano-structures of silica can thus

C. Tank · S. Gosavi · S. V. Bhoraskar · V. L. Mathe (✉)
Department of Physics, University of Pune, Pune 411007, India
e-mail: vlmathe@physics.unipune.ac.in

S. Raman · W. N. Gade
Department of Biotechnology, University of Pune,
Pune 411007, India

S. Karan · R. Berndt
Institut für Experimentelle und Angewandte Physik,
Christian-Albrechts-Universität zu Kiel, 24098 Kiel,
Germany

N. P. Lalla · V. Sathe
UGC-DAE Consortium for Scientific Research, University
Campus, Khandwa Road, Indore 52017, India

provide very useful antimicrobial properties to polymers [11]. Song et al. [12] have reported antimicrobial studies of silica nano-particles modified by polymer whereas Hebalkar et al. [13] have reported the synthesis of silica nano-particles for antibacterial and self-cleaning surfaces. Nano-particles of silica are used in biological applications [14, 15] as scaffolds for drug delivery by functionalizing their surfaces and attaching biomolecules [16]. Likewise, nanoparticles of silica are used to form composites with metal nanoparticles like silver to avoid their aggregation and hence enhance antibacterial activity [17]. They are also important with regard to dental applications, mainly fillings [18].

Furthermore, nano-silica showing a hollow structure is considered superior to solid structures, as hollow nano-structures possess a greater effective surface area. They are expected to provide the increased effective surface reactivity needed for charge accumulation, which can contribute to antimicrobial activity. Several methods, like pulsed laser ablation [19], chemical vapor deposition [20], and the template method involving sol–gel techniques [21, 22], have been reported for the synthesis of silica nanotubes. Most of these methods involve the use of harmful chemicals like silane and silane derivatives and some are catalyst dependent. Moreover, silica nanotubes synthesized by these methods have a wall thickness of the order of several nanometers. We present our work on the synthesis of silica-coated silicon nanoparticles (SCSNPs), and silica-coated thin-walled silicon nanotubes using catalyst-free thermal plasma-assisted gas phase condensation technique. Thermal plasma synthesis has the advantage of being a clean process which ensures a high yield [23]. It produces highly crystalline products that are free of contaminants, as it is a high temperature process. In addition, synthesized nanotubes have a wall thickness of less than one nanometer, which is rarely reported. The morphology and structure of silicon nano-structures was analyzed using transmission electron microscopy (TEM), scanning tunneling microscopy (STM) and Raman spectroscopy.

The antimicrobial activity of as synthesized nano-structures was studied for selected strains of bacteria which are pathogenic and frequently colonize medical devices. The Gram-positive bacteria included were *Bacillus subtilis* and *Staphylococcus aureus*, whereas Gram-negative bacteria were *Escherichia coli* and *Pseudomonas aeruginosa*. *S. aureus* is one of the major resistant pathogens found on the mucous membranes and human skin of around one-third of the population and it is very adaptable to antibiotics [24]. The antibacterial activity was assayed using the optical densitometry technique and viable cell counting method, using plating technique. Here we report the synthesis, antimicrobial activity and the potential use of ultra thin walled silica-coated silicon nano-structures in the formulation of new types of bactericidal materials.

2 Experimental details

2.1 Synthesis of nano-particles and nano-tubes

The nano-structures of silicon consisted mainly of nanoparticles and nanotubes, and these were synthesized in a DC arc plasma reactor. The plasma reactor consisted of a graphite anode (in the form of a crucible) and a tungsten cathode (in the form of a 4 mm diameter rod) mounted in a vertical geometry. The electrode system was housed inside a double-walled, water-cooled stainless steel chamber. The silicon powder, from CDH, India Ltd., was placed in the graphite anode. The schematics of the plasma reactor and the detailed morphological analysis of silica-coated, silicon nanotubes (SCSNTs) have been included in our earlier publications [23, 25]. The chamber was pre-evacuated to a base pressure of about 10^{-3} mbar and was filled with the desired gas to maintain a pressure of 700 mbar during arcing. The arc voltage and arc current were maintained at about 12 ± 0.4 V and 80 ± 5 A respectively. In such a reactor arcing generates a plasma plume, which produces heat that causes melting and evaporation of the anode material. Homogeneous nucleation of the evaporated atoms occurs on account of the steep temperature gradient outside the plasma plume. However, growth is restricted due to a high collision rate resulting from a high partial pressure of the inert gas that prevails in the chamber. The resulting nanoparticles then condense and are collected from the walls of the chamber.

Two batches of samples consisting of nano-silicon were prepared in the presence of (a) 100 % Ar gas and (b) 95 % Ar + 5 % H₂ gas. The main constituents of batch 'a' and batch 'b' were SCSNPs and SCSNTs respectively.

2.2 Characterization of as synthesized nano-structures

The samples were dispersed in methanol and were coated on a holey carbon-coated copper grid for TEM analysis using a Technai G² 20 microscope, facilitated by a LaB₆ filament and a charge coupled device (CCD) camera. Nanotubes were further studied by OMICRON STM in an ultra high vacuum (UHV) at room temperature. The elemental purity was revealed by energy dispersive X-ray (EDX) analysis in a scanning electron microscope (SEM) (JEOL model JSM-6360A). Raman spectra were recorded in a backscattering geometry at room temperature, using a Jobin-Yvon Labram HR800 spectrometer with a He–Ne laser ($\lambda = 632.81$ nm) for excitation. The effective surface area measurements were carried out by the nitrogen adsorption process in a single-point Brunauer, Emmett and Teller (BET) instrument (Smart Sorb 91 model).

2.3 Microbial strains and culture media

The bacterial strains were procured from the National Collection of Industrial Microorganisms (NCIM), India.

The Gram-positive bacterial strains tested were *S. aureus* (NCIM 2079) and *B. subtilis* (NCIM 2063). The Gram-negative strains used were *E. coli* (NCIM 2065) and *P. aeruginosa* (NCIM 2200). The above bacterial strains were cultured in Nutrient Broth (NB) media (10 g yeast extract, 5 g sodium chloride, 10 g tryptone and 20 g Agar in one litre media with the pH maintained between 7 and 7.5). *B. subtilis* were pre-inoculated in 2 ml of NB media and grown at 30 °C overnight while all other bacteria were grown at 37 °C overnight. Except for *B. subtilis*, the population of microbes was maintained between 1×10^8 and 5×10^9 CFU/ml.

2.4 Antibacterial test

2.4.1 Estimation of minimum inhibitory concentration (MIC) using the optical densitometric technique

The micro dilution method was used for estimating the MIC of the samples to determine the antibacterial activity. The colloidal solutions of SCSNPs and SCSNTs, with a concentration of 1 mg/ml were prepared by ultrasonating them with distilled water for 30 min. The experimental miniprep consisted of 900 μ l of NB media, 100 μ l of respective bacterial inoculums and silicon nano-structures in various concentrations (0, 10, 50, 100, 150 and 200 μ g/ml). Sterile, distilled water equal to the reaction volume was added. *B. subtilis* were allowed to grow overnight at 30 °C and the rest of the strains were incubated at 37 °C overnight. Each and every test sample along with the control, was diluted up to 10^9 dilutions using 0.9 % sodium chloride (saline).

To determine the MIC values 100 μ l of all the tested concentrations of inoculums, and their dilutions up to 10^9 were added to 96 wellplates. Optical absorbance at 600 nm was then recorded in an enzyme-linked immune sorbant assay (ELISA) reader (Thermo Scientific Multiskan EX). NB media was used as a negative control. 100 μ l of the experimental mixture without SCSNPs and SCSNTs, was used as a positive control. Optical absorbances for both SCSNPs and SCSNTs at different concentrations without bacterial inoculums, along with their dilutions up to 10^9 in saline, were also recorded.

2.4.2 Determination of colony forming units (CFU)

From the above experimental miniprep, 100 μ l of the sample was used from each test concentration, with dilutions of 10^9 , 10^8 and 10^7 , to plate the bacterial inoculums, including the control. In *B. subtilis* the plating was carried out in dilutions of 10^5 , 10^4 and 10^3 owing to the low optical density. The CFU were determined by counting the bacterial colonies and then multiplying this with the dilution factor. All assays were carried out in duplicate.

3 Results and discussion

3.1 Characterization of nano-structures

3.1.1 BET measurements

The prime contribution of these nano-structures seems to arise from the large specific surface area that was estimated by the nitrogen absorption method using BET. The measured values were found to be 300 and 100 m²/g for SCSNPs and SCSNTs respectively.

3.1.2 TEM analysis

The morphological information was obtained from the TEM analysis. Figure 1a shows the TEM image of the sample: SCSNP, while Fig. 1b shows the TEM micrographs of the sample: SCSNT. Figure 1a shows the presence of surface-oxidized spherical silicon nano-particles, with sizes varying from 5 to 60 nm. In addition, it also consists of some fiber-like structures in a small proportion. The TEM micrograph of SCSNT (Fig. 1b) reveals that the sample contains nanotubes as well as nanoparticles. The nanotubes appear in bundles wound around each other, along with some nanoparticles of silicon. The nanotubes and nanoparticles are seen to be in the ratio of $\sim 70:30$. The nanoparticles are spherical in shape, with sizes varying in the range 5–25 nm, while the diameters of the nanotubes range between 9 and 30 nm. A large number of tubes have a diameter of 14 ± 2 nm, while their lengths are in the order of several hundreds of nanometers. Tubular formation is apparent from the circular open tip of a single nanotube as shown in the inset of Fig. 1b. The inner part of the nanotube appears homogeneously bright. At its tip the hollow opening is clearly visible. The thickness of the annular dark wall seen at the tip happens to be less than 1 nm. The dark lines running along the lengths at the two edges of the nanotubes appear to have a similar thickness. The thickness of the nanotube is equivalent to two or three monolayers of buckled Si (111) planes. Such nanotubes must have been formed by the rolling of planar sheets of silicon in a buckled geometry. The accuracy of the measurement is limited, and so the exact confirmation cannot be made.

3.1.3 STM analysis

The adsorption geometry of these tubular structures on an atomically flat surface was analyzed by STM. Figure 2a shows the STM image of a single silicon nanotube adsorbed on a freshly cleaved, highly oriented, pyrolytic graphite (HOPG) surface. Almost every nanotube found during the experiment showed a fairly small topographic height compared to its diameter as shown in the line profile (Fig. 2b) recorded along the marked line in Fig. 2a. Such a

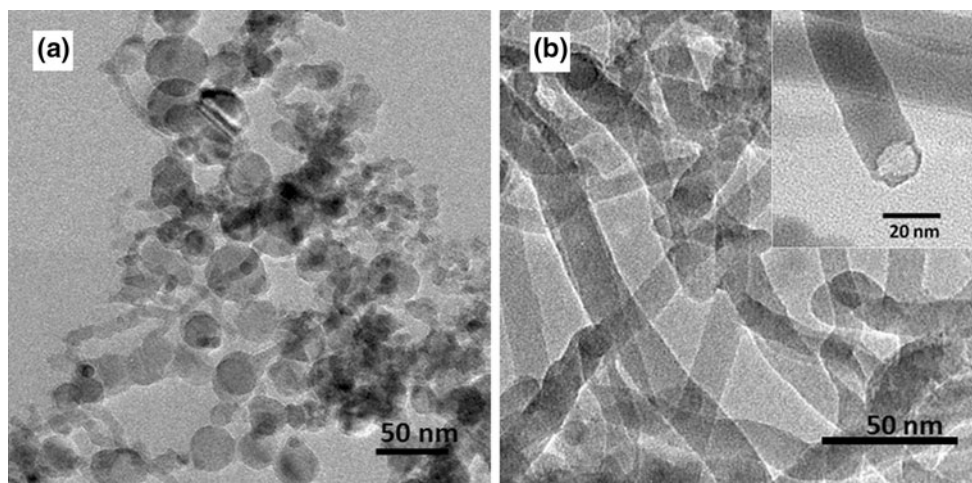


Fig. 1 Transmission electron micrograph of silicon nano-structures: **a** TEM of SCSNPs and **b** TEM of SCSNTs. *Inset* shows TEM image of the tip of a nano-tube

discrepancy occurs mainly due to the geometrical convolution between the STM tip shape and the nanotubes [26, 27]. However, the dependence of the tunneling gap [28, 29] on local conductivity should also be considered. For example, fullerene C_{60} appears almost 40 % lower than its actual height in the STM topography, even with a single atom at the apex of the STM tip. Thus, it is not easy in general to obtain the real geometry of the tube adsorbed on the substrate. From the line profile, we estimated [30] the tube diameter, with some errors approximately 11 nm, while the lower limit of the estimated height is 1.4 nm. This indicates that a strong radial compression of the nanotube is induced by van der Waals interaction between the tube and the substrate. A similar kind of radial compression occurs for carbon nanotubes in the case of less number of shells or a single wall [31] contrary to multiwall tubes. So, the tubes studied are possibly few layered or single-walled structures.

3.1.4 SEM–EDX analysis

Further studies using SEM–EDX provide evidence for the presence of oxygen in both samples. Figure 3a, b shows the SEM–EDX spectra for samples of SCSNPs and SCSNTs respectively. The spectrum shows peaks at 0.525, 0.129 and 1.739 keV, which correspond to O K_{α} , Si $L_{2,3}$ and Si K_{α} edge respectively. It is observed that the ratio of silicon to oxygen for SCSNPs is 0.88 whereas it is 1.27 for SCSNTs.

3.1.5 Raman spectroscopic analysis

The presence of crystalline silicon was studied, using Raman spectroscopy. Figure 4a–c shows the Raman spectra for crystalline silicon, SCSNT and SCSNP, respectively.

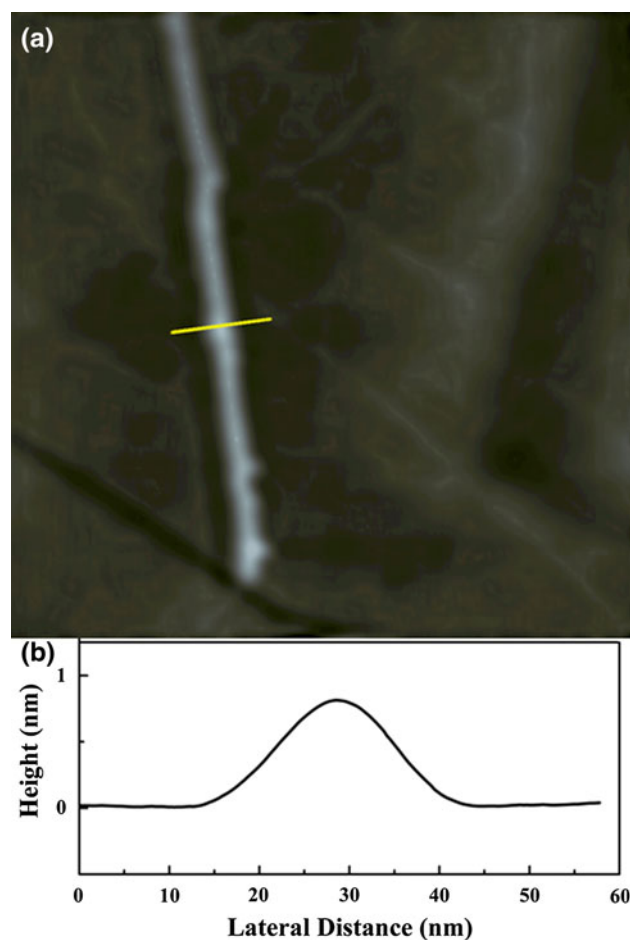


Fig. 2 **a** STM image ($360 \times 360 \text{ nm}^2$) of single silicon nano-tube on HOPG; $V_{\text{bias}} = 1 \text{ V}$, $I_{\text{tunn}} = 0.95 \text{ nA}$. **b** Line profile along the yellow line drawn in **a** (Color figure online)

The peak for crystalline silicon is found to be symmetric and appears at 520.5 cm^{-1} , with the full width at half

Fig. 3 SEM–EDX profiles of silicon nano-structures: **a** SEM–EDX profile of SCSNPs and **b** SEM–EDX profile of SCSNTs

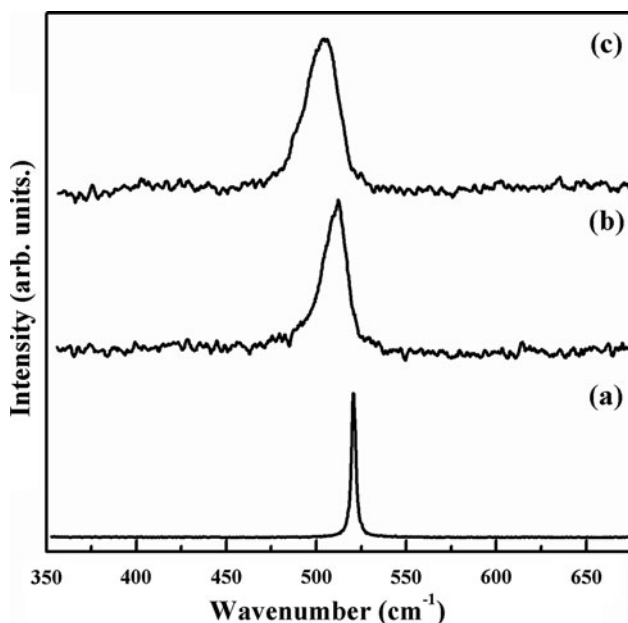
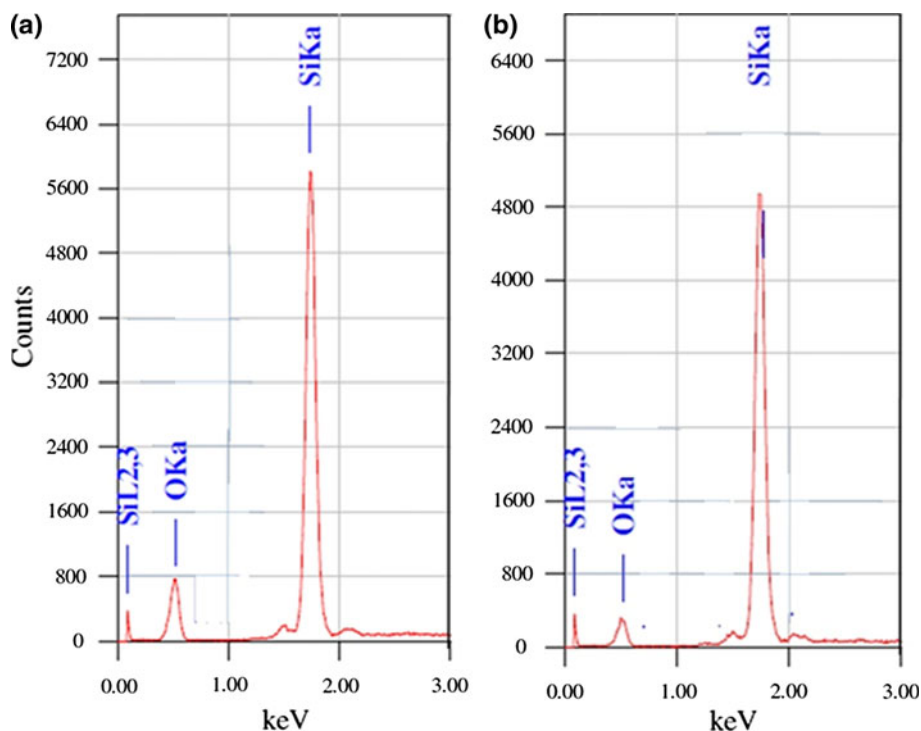


Fig. 4 Raman spectra of silicon (a) Raman spectra of crystalline silicon, (b) Raman spectra of SCSNTs and (c) Raman spectra of SCSNPs

maximum (FWHM) of the peak being 2.8 cm^{-1} . Figure 4b shows an asymmetric peak at 511.5 cm^{-1} with a FWHM of 15.8 cm^{-1} for SCSNT. An asymmetric peak is also observed in Fig. 4c at 504 cm^{-1} with a FWHM of 22 cm^{-1} . These peaks are red-shifted as compared to bulk silicon and have an asymmetric nature, which can be attributed to the

phonon confinement effect in the nano-structures. The peak for the nanotube-rich sample, i.e., SCSNT is red-shifted by 9 cm^{-1} , while that for the nanoparticles-rich sample, i.e., SCSNP by 16.5 cm^{-1} . This can be attributed to the two-directional phonon confinement in the case of nanotubes, and to the three-dimensional confinements in nanoparticles.

The Raman spectroscopic analysis thus confirms that silicon nanotubes as well as silicon nanoparticles are crystalline in nature whereas EDX analysis has shown that their surface has oxide layers. Furthermore, it has been inferred that the walls of these hollow nano-structures, made of silicon and silicon oxide, are extremely thin. Oxygen is present on the surface of the nanotubes, and since it has a higher electro-negativity than silicon it attracts the bonded pair of electron towards itself. Thus, oxygen acquires partial negative charge. When many such oxygen atoms come close to each other, it gives rise to surface charging effects, which are usually observed in silica. In the present case, the oxide layer, being ultra-thin will have a tendency to accumulate a higher charge density on its surface, and this could possibly be the reason for antibacterial activity.

3.2 Antibacterial activity

3.2.1 Optical densitometric analysis

The values of MIC for SCSNPs and SCSNTs were obtained from measurements of optical density at 600 nm for the inoculums containing different bacteria. These are

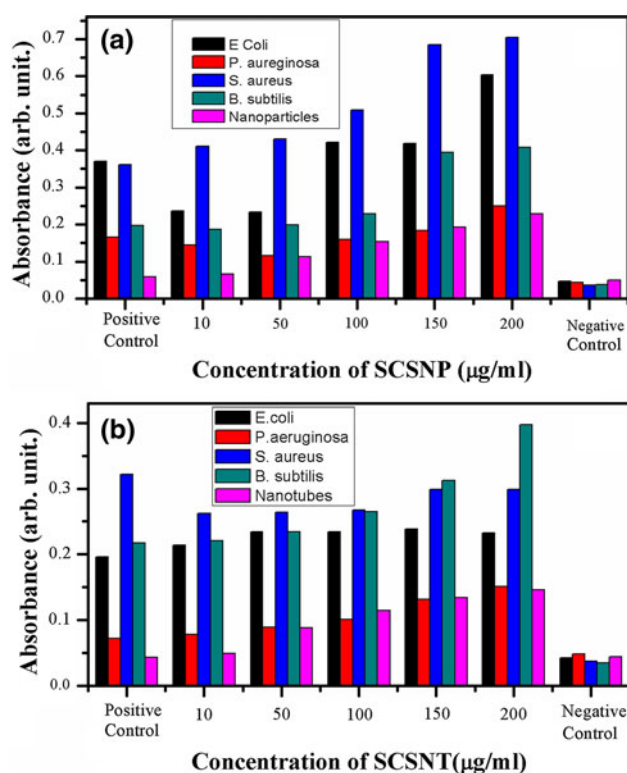


Fig. 5 Effect of different concentrations of silicon nano-structures on bacterial strains tested. Standard absorbance values of silicon nano-structures at various concentrations from 0 µg/ml (positive control) to 200 µg/ml are provided. Experimental mixture having NB media with respective bacterial inoculums, without nano-structures was used as *positive control*. NB media alone was used as *negative control*. **a** Effect of SCSNPs on bacterial strains tested and **b** effect of SCSNTs on bacterial strains tested

shown in Fig. 5a, b. There are certain limitations associated with using optical density techniques to determine bacterial viability in the presence of nano-materials since the latter themselves contribute to optical density at different concentrations [32]. To resolve this issue, optical densities of the nano-structures, SCSNPs and SCSNTs, are given along with the other data for reference.

We found that the concentration of nano-particles at which the growth was inhibited was different for different bacteria. In SCSNP treatment the growth of *E. coli* and *B. subtilis* was inhibited at 10 µg/ml, while for *P. aeruginosa*, inhibition was observed at 50 µg/ml. *S. aureus* did not show any inhibition with the use of SCSNPs. In contrast, SCSNTs showed an MIC of 10 µg/ml for *S. aureus*. The IC-50 value is found to be 100 µg/ml. Reports from “The Center for Disease Control and Prevention” indicate that the number of annual multidrug-resistant *S. aureus* (MRSA) infections increased from 127,000 to 278,000 between 1999 and 2005 [32]. In this scenario, SCSNTs would be a potential candidate to target MRSA infections. The inhibition of *E. coli* and *P. aeruginosa* by SCSNTs is

comparable to SCSNPs. In contrast to SCSNPs, the growth of *B. subtilis* cultures were not inhibited by SCSNTs. Thus, the data demonstrates the difference in the mechanism of inhibition of bacterial strains by these two nano-structures.

The inhibition generally occurs due to inhibition of reactive oxygen species, membrane disruption, protein inactivation, flocculation or other unknown mechanisms [32]. Further studies need to be carried out to understand the mechanism of inhibition by these nano-structures (SCSNPs and SCSNTs). The MIC was found to be of the order of micrograms for these tested nano-materials, which is comparable to those reported in metal oxides for both Gram-positive as well as Gram-negative bacteria [32]. In many cases, the MIC values obtained for silica nano-structures are better than those reported in other oxide systems [32].

3.2.2 CFU analysis

In order to measure the viable cells, CFU were determined by using serial dilutions of suspensions, followed by spread-plate colony counting. When exposed to different concentrations of SCSNPs, *B. subtilis* showed a reduced viability at 100 µg/ml (Fig. 6a), whereas an increased viability is observed at 200 µg/ml. This may be attributed to the interaction of SCSNPs with bacteria at high concentrations. The *B. subtilis* cultures, exposed to SCSNTs, showed a definite pattern of reduced viability (Fig. 6b), with an increase in SCSNTs concentration although initial optical densitometry analysis could not clearly discern inhibition (Fig. 5b). The IC-50 value of SCSNTs was 200 µg/ml in *B. subtilis* cultures.

In *S. aureus* (Fig. 6c), the IC-50 value was found to be 100 µg/ml for SCSNPs. However, the optical densitometric analysis could not reveal the inhibition (Fig. 5a), possibly due to interference by the optical activity of SCSNPs. The 10 µg/ml of SCSNTs proved to be effective in controlling the *S. aureus* even at very low concentrations with an IC-50 value of 100 µg/ml (Fig. 6d). Although nano-materials like ZnO [33], Fe₃O₄ [34] and Ag particles proved to be effective against MRSA infection, SCSNTs proved to be effective even at very low concentrations (10 µg/ml). Thus, the biocompatible nature and cost-effective, eco-friendly synthesis add to the efficacy of thin-walled, SCSNTs as an effective antibacterial agent.

With Gram-negative bacteria like *E. coli*, the MIC was found to be 10 µg/ml for both SCSNPs and SCSNTs, which concurs with densitometric analysis (Fig. 7a, b). A definite pattern of inhibition as the concentration increases was observed in both SCSNPs and SCSNTs. In *P. aeruginosa*, 50 µg/ml was found to be effective in reducing the viability in both SCSNPs and SCSNTs (Fig. 7c, d). Thus, SCSNPs and SCSNTs are found to be effective in controlling both the Gram-positive and Gram-negative bacterial strains that were tested.

Fig. 6 CFU counting in Gram-positive bacterial strains calculated for different concentrations of nano-structures (0–200 µg/ml). **a** CFU of *B. subtilis* cultures calculated at the dilutions of 10^3 , 10^4 and 10^5 for SCSNPs. **b** CFU of *B. subtilis* cultures calculated at the dilutions of 10^3 , 10^4 and 10^5 for SCSNTs. **c** CFU of *S. aureus* cultures calculated at the dilutions of 10^7 , 10^8 and 10^9 for SCSNPs. **d** CFU of *S. aureus* cultures calculated at the dilutions of 10^7 , 10^8 and 10^9 for SCSNTs

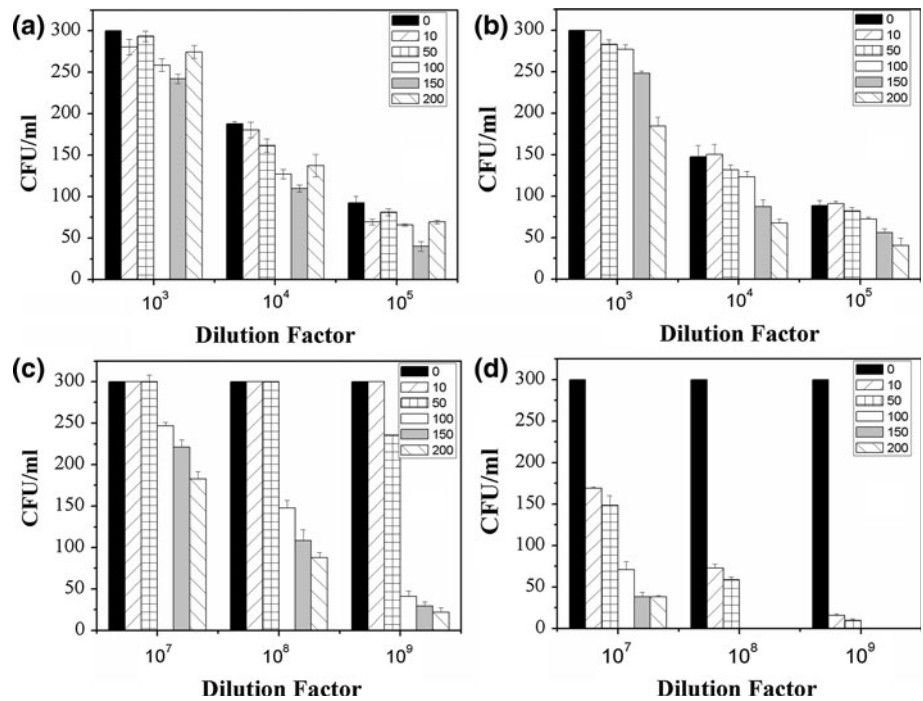
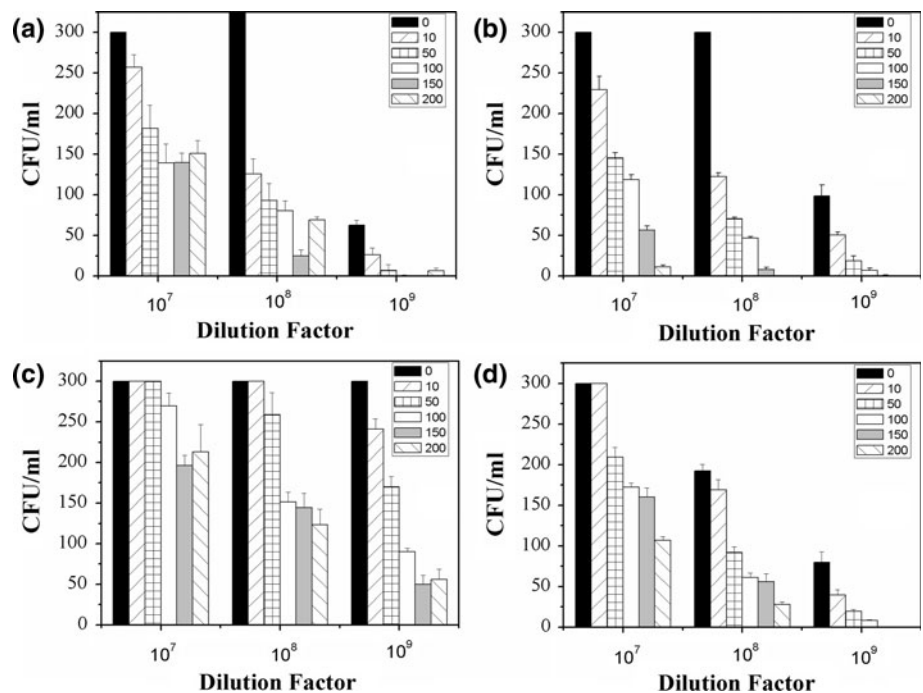


Fig. 7 CFU counting in Gram-negative bacterial strains calculated at the dilutions of 10^7 , 10^8 and 10^9 for different concentrations of nano-structures (0–200 µg/ml). **a** CFUs of *E. coli* cultures for SCSNPs. **b** CFU of *E. coli* cultures for SCSNTs. **c** CFU of *P. aeruginosa* cultures for SCSNPs. **d** CFU of *P. aeruginosa* cultures for SCSNTs



4 Conclusions

We have shown that the growth of thin walled nano-tubes (<1 nm) is enabled by thermal plasma-assisted, gas phase condensation, which is a clean method of synthesis. The possibility of synthesizing metastable states increases in this method due to the high processing temperature and

steep temperature gradient. In addition, we have shown that silica-coated silicon nano-structures can be a good substitute as a cheaper and biocompatible antimicrobial agent. The low values of MIC are encouraging, and indicate the specific surface properties of the silicon nano-structures. It is proposed that due to the extremely thin oxide layers of silicon nano-structures, their interaction with the bacteria is

strong and capable of inhibition. In this study we emphasize the important role of SCSNTs in controlling MRSA infections, thus making them an efficient antiMRSA agent.

Acknowledgments The authors would like to thank the Council of Scientific & Industrial Research (CSIR), India, for their financial support under the emeritus scientist scheme and senior research fellowship. We also acknowledge the Board of Research in Nuclear Science (BRNS), India for funding the project.

References

- Mongillo JF. Nanotechnology in medicine and health. In: Mongillo JF, editor. Nanotechnology 101. Goleta: ABC-CLIO; 2007. p. 103–24.
- Salata O. Applications of nano-particles in biology and medicine. *J Nanobiotech*. 2004;2:3.
- Chitravadivu C, Manian S, Kalaichelvi K. Antimicrobial studies on selected medicinal plants, Erode region, Tamilnadu, India. *Middle-East J Sci Res*. 2009;4:147–52.
- Rai A, Prabhune A, Perry CC. Antibiotic mediated synthesis of gold nano-particles with potent antimicrobial activity and their application in antimicrobial coatings. *J Mater Chem*. 2010;20:6789–98.
- Beck R, Guterres S, Pohlmann A. *Nanocosmetics and nanomedicines: new approaches for skin care*. 1st ed. New York: Springer; 2011.
- Seil JT, Webster TJ. Zinc oxide nanoparticle and polymer antimicrobial biomaterial composites. In: Bioengineering conference, proceedings of the 2010 IEEE 36th annual northeast. Washington, DC: IEEE; 2010. p. 1–2.
- Liu P. Facile preparation of monodispersed core/shell zinc oxide@polystyrene (ZnO@PS) nano-particles via soapless seeded microemulsion polymerization. *Colloids Surf A*. 2006;291:155–61.
- Lok C, Ho C, Chen R, He Q, Yu W, Sun H, Tam PK, Chiu J, Che C. Silver nano-particles: partial oxidation and antibacterial activities. *J Biol Inorg Chem*. 2007;12:527–34.
- Levard C, Hotze EM, Lowry GV, Brown GE Jr. Environmental transformations of silver nanoparticles: impact on stability and toxicity. *Environ Sci Technol*. 2012;46:6900–14.
- Sambhy V, MacBride MM, Peterson BR, Sen A. Silver bromide nanoparticle/polymer composites: dual action tunable antimicrobial materials. *J Am Chem Soc*. 2006;128:9798–808.
- Xia X, Shurong L, Fayun J, Pu L. Synthesis and antimicrobial activity synthesis and antimicrobial activity of nano-fumed silica derivative with *N,N*-dimethyl-*n*-hexadecylamine. *Life Sci J*. 2006;3:59–62.
- Song J, Kong H, Jang J. Enhanced antibacterial performance of cationic polymer modified silica nano-particles. *Chem Commun* 2009;5418–5420.
- Hebalkar NY, Acharya S, Rao TN. Preparation of bi-functional silica particles for antibacterial and self cleaning surfaces. *J Colloid Interface Sci*. 2011;364:24–30.
- Nakamura M, Shono M, Ishimura K. Synthesis, characterization, and biological applications of multifluorescent silica nano-particles. *Anal Chem*. 2012;79:6507–14.
- Egger S, Lehmann RP, Height MJ, Loessner MJ, Schuppler M. Antimicrobial properties of a novel silver–silica nanocomposite material. *Appl Environ Microbiol*. 2009;75:2973–6.
- Trewyn BG, Whitman CM, Lin VS-Y. Morphological control of room-temperature ionic liquid templated mesoporous silica nanoparticles for controlled release of antibacterial agents. *Nano Lett*. 2012;4:2139–43.
- Zhanga X, Niu H, Yanb J, Caia Y. Immobilizing silver nanoparticles onto the surface of magnetic silica composite to prepare magnetic disinfectant with enhanced stability and antibacterial activity. *Colloids Surf A*. 2011;375:186–92.
- Lühns A-K, Geurtsen W. The application of silicon and silicates in dentistry: a review. *Prog Mol Subcell Biol*. 2009;47:359–80.
- Yang Y, Wu S, Chiu H, Lin P, Chen Y. Catalytic syntheses of silicon nanowires and silica nanotubes. In: 4th IEEE conference on nanotechnology, Munich; 2004. p. 448–50.
- Li R, Zhang Y, Zhou X, Sun X. Silica nanotubes decorated with internal periodic rings. *Chem Phys Lett*. 2008;458:138–42.
- Yu Y, Qiu H, Wu X, Li H, Li Y, Sakamoto Y, Inoue Y, Sakamoto K, Terasaki O, Che S. Synthesis and characterization of silica nanotubes with radially oriented mesopores. *Adv Funct Mater*. 2008;18:541–50.
- Yin Z-H, Liu X, Su Z-X. Novel fabrication of silica nano-tubes using multi-walled carbon nano-tubes as template. *Bull Mater Sci*. 2010;33:351–5.
- Bhoraskar SV, Tank CM, Mathe VL. Thermal plasma assisted synthesis of nanocrystalline silicon—a review. *Nanosci Nanotechnol Lett*. 2012;4:291–308.
- Maple PA, Hamilton-Miller JM, Brumfitt W. World-wide antibiotic resistance in methicillin-resistant *Staphylococcus aureus*. *Lancet*. 1989;1:537–40.
- Castrucci P, Diociaiuti M, Tank CM, Casciardi S, Tombolini F, Scarselli M, De Crescenzi M, Mathe VL, Bhoraskar SV. Si nanotubes and nanospheres with two-dimensional polycrystalline walls. *Nanoscale*. 2012;4:5195–201.
- Biró LP, Lazarescu S, Lambin P, Thiry PA, Fonseca A, Nagy JB, Lucas AA. Scanning tunneling microscope investigation of carbon nano-tubes produced by catalytic decomposition of acetylene. *Phys Rev B*. 1997;56:12490–8.
- Zha F-X, Czerw R, Carroll DL, Kohler-Redlich P, Wei B-Q, Loiseau A, Roth S. Scanning tunneling microscopy of chromium-filled carbon nano-tubes: tip effects and related topographic features. *Phys Rev B*. 2000;61:4884–9.
- Tersoff J, Hamann DR. Theory and application for the scanning tunneling microscope. *Phys Rev Lett*. 1983;50:1998–2001.
- Zha F-X, Carroll DL, Czerw R, Loiseau A, Pascard H, Claus W, Roth S. Electronic effects in scanning tunneling microscopy of dendritic, Cr-filled carbon Nano-tubes. *Phys Rev B*. 2001;63:165432-1–5.
- Park MH, Jang JW, Lee CE, Lee CJ. Interwall support in double-walled carbon nano-tubes studied by scanning tunneling microscopy. *Appl Phys Lett*. 2005;86:023110-1–3.
- Hertel T, Walkup RE, Avouris P. Deformation of carbon nanotubes by surface van der Waals forces. *Phys Rev B*. 1998;58:13870–3.
- Seil TJ, Webster TJ. Antimicrobial applications of nanotechnology: methods and literature. *Int J Nanomed*. 2012;7:2767–81.
- Kallen AJ, et al. Health care-association invasive MRSA infections, 2005–2008. *J Am Med Assoc*. 2010;304:642–8.
- Jones N, Ray B, Ranjit KT, Manna AC. Antibacterial activity of ZnO nanoparticle suspensions on a broad spectrum of microorganisms. *FEMS Microbiol Lett*. 2008;279:71–6.